Journal of Geophysical Research: Solid Earth

Supporting Information for

Numerical Modelling of Coupled Climate, Tectonics and Surface Processes on the Eastern Himalayan Syntaxis

Xueyun Lu[1], Jingtao Lai[2], Lining Wang[3,4], Jianqing Ji[1], Dalai Zhong[5]

[1]Key Laboratory of Orogenic Belts and Crustal Evolution, School of Earth and Space Sciences, Peking University, Beijing 100871, China

[2]Earth Surface Process Modelling, GFZ German Research Centre for Geosciences, 14473 Potsdam, Germany

[3]Research Institute of Petroleum Exploration & Development, PetroChina, Beijing 100083, China

[4]Key Laboratory of Basin Structure & Hydrocarbon Accumulation, CNPC, Beijing 100083, China

[5]Institute of Geology and Geophysics, Chinese Academy of Sciences, Beijing 100029, China

Contents of this file

Introduction

This supporting information provides supplemental Texts S1 and S2 describing the visco-elasto-plastic rheology of rocks and the partial melting model included in our thermomechanical model, respectively. Text S3 presents the details regarding the selection of parameters α_P and β_P in the orographic precipitation model (Equation (9) in the main text). Supplemental Figure S1 shows the testing results of the sensitivity of predicted precipitation to the parameters α_P and β_P based on the orographic precipitation model. Supplemental Table S1 presents the material properties used in the numerical experiments. Tables S2 to S4 are numerical experiment summaries in this study.

Text S1. Visco-elasto-plastic rheology

The deformation behavior of rocks in this study is considered visco-elasto-plastic, and the bulk deviatoric strain rate $\dot{\varepsilon}'_{ij}$ can be decomposed into three respective components:

$$\dot{\varepsilon}'_{ij} = \dot{\varepsilon}'_{ij(viscous)} + \dot{\varepsilon}'_{ij(elastic)} + \dot{\varepsilon}'_{ij(plastic)} \quad (1)$$

while

$$\dot{\varepsilon}'_{ij(viscous)} = \frac{1}{2\eta_{cr}}\sigma'_{ij} \quad (2)$$

$$\dot{\varepsilon}'_{ij(elastic)} = \frac{1}{2\mu}\frac{\widehat{D}\sigma'_{ij}}{Dt} \quad (3)$$

$$\dot{\varepsilon}'_{ij(plastic)} = 0 \; for \; \sigma_{\mathrm{II}} < \sigma_{yield} \quad (4)$$

$$\dot{\varepsilon}'_{ij(plastic)} = \chi\frac{\partial G_{plastic}}{\partial \sigma'_{ij}} = \chi\frac{\sigma'_{ij}}{2\sigma_{\mathrm{II}}} \; for \; \sigma_{\mathrm{II}} = \sigma_{yield} \quad (5)$$

where μ is the shear modulus, $\frac{\widehat{D}\sigma'_{ij}}{Dt}$ is the objective co-rotational time derivative of the deviatoric stress component σ'_{ij}, $G_{plastic}$ is the plastic flow potential, σ_{yield} is the plastic yield strength for a given rock, $\sigma_{\mathrm{II}} = \sqrt{\frac{1}{2}{\sigma'_{ij}}^2}$ is the second invariant of the deviatoric stress tensor, χ is the plastic multiplier, η_{cr} is the viscosity for viscous creep of rocks (ductile flow), and it depends on temperature, pressure and strain rate(Ranalli, 1995):

$$\eta_{cr} = \frac{\dot{\varepsilon}_{\mathrm{II}}^{(1-n)/n}}{A_D^{1/n}} e^{\frac{E_a+PV_a}{nRT}} \quad (6)$$

where $\dot{\varepsilon}_{\mathrm{II}} = \sqrt{\frac{1}{2}{\dot{\varepsilon}_{ij}}^2}$ is the second invariant of the strain rate tensor, A_D, n, E_a and V_a are experimentally determined flow law parameters, which represent material constant, stress exponent, activation energy and activation volume, respectively. R is the gas constant.

The plasticity is implemented using the following yield criterion (Gerya, 2019):

$$\sigma_{yield} = \sigma_c + \gamma_{int}P \quad (7)$$

It is assumed that the local plastic strength of rocks depends on the dynamic pressure (P). σ_c is the compressive strength, and its relationship with the material cohesion(c) is given by $\sigma_c = c\cos(\varphi)$. Here φ is the angle of internal friction. $\gamma_{int} = \sin(\varphi)$ is the internal friction coefficient.

Text S2. Partial melting

The thermomechanical model accounts for partial melting of the various lithologies by using experimentally obtained P-T dependent wet solidus and dry liquidus curves. In this simple partial melting model, the volumetric fraction of melt M at a certain pressure is assumed to increase linearly with temperature according to the relations (Burg & Gerya, 2005; Gerya & Yuen, 2003):

$$M = 0 \; at \; T \le T_{solidus}$$

$$M = \frac{(T - T_{solidus})}{(T_{liquidus} - T_{solidus})} \; at \; T_{liquidus} < T < T_{solidus} \quad (8)$$

$$M = 1 \; at \; T \ge T_{liquidus}$$

where $T_{solidus}$ and $T_{liquidus}$ are the wet solidus and dry liquidus temperatures of the considered rock, respectively. For the rocks with partial melt fraction M greater than 0.1, their effective viscosity η_e is calculated according to the following formula (Bittner & Schmeling, 1995; Pinkerton & Stevenson, 1992):

$$\eta_e = \eta_0 exp\left[2.5 + (1-M)\left(\frac{1-M}{M}\right)^{0.48}\right] \quad (9)$$

here η_0 is an empirical parameter depending on rock types. For partially molten mafic rocks, it can be set to $10^{13}\ Pa\ s$ (i.e.,$1 \times 10^{14} \leq \eta_e \leq 2 \times 10^{15}\ Pa\ s\ for\ 0.1 \leq M \leq 1$), and for felsic rocks, $\eta_0 = 5 \times 10^{14}\ Pa\ s$(i.e.,$6 \times 10^{15} \leq \eta_e \leq 8 \times 10^{16}\ Pa\ s\ for\ 0.1 \leq M \leq 1$) can be adopted (Bittner & Schmeling, 1995).

For the partially molten rocks, their effective density (ρ_e) is then calculated from:

$$\rho_e = \rho_{solid}\left(1 - M + M\frac{\rho_{0(molten)}}{\rho_{0(solid)}}\right) \quad (10)$$

where $\rho_{0(solid)}$ and $\rho_{0(molten)}$ are the standard densities of solid and molten rock, respectively. ρ_{solid} is the density of solid rocks at given pressure (P) and temperature (T), and it's computed as:

$$\rho_{solid} = \rho_r[1 + \beta(P - P_r)] \times [1 - \alpha(T - T_r)] \quad (11)$$

where α is thermal expansion, β is compressibility, ρ_r is the density of a specific material at reference pressure P_r (typically $10^5\ Pa$) and temperature T_r (273 K).

The effect of latent heating due to equilibrium melting/crystallization are accounted for by increasing the effective heat capacity($C_{P(eff)}$) and the thermal expansion(α_{eff}) of partially melting/crystallization rocks($0 < M < 1$), calculated as (Burg & Gerya, 2005):

$$C_{P(eff)} = C_p + Q_L\left(\frac{\partial M}{\partial T}\right)_{P=const} \quad (12)$$

$$\alpha_{eff} = \alpha + \rho\frac{Q_L}{T}\left(\frac{\partial M}{\partial P}\right)_{T=const} \quad (13)$$

where C_p is the heat capacity of the solid rock and Q_L is the latent heat of melting of the rock.

Text S3. The selection of parameters α_P and β_P

To gain better insight into and select reasonable values for the parameters α_P and β_P, we firstly tested the sensitivity of predicted precipitation to the parameters α_P and β_P based on Equation (9) in the main text (Figure S1). From the testing results, it can be observed that this model (Equation (9) in the main text) is capable to capture the primary characteristics of the pattern of orographic precipitation, especially the local precipitation enhancement on the windward side and the rain shadow on the leeward side. However, it tends to overestimate the precipitation in the inland areas on the right side (leeward side) of the mountain ranges. This is largely due to the fact that in this model, the distinction between the windward and leeward sides is determined solely by the sign of the topographic slope. However, for most cases of simulating convergent plate boundary settings, the areas on both sides of the convergence center are usually vast plains where the erosional potential approaches zero. Therefore, the impact on erosion patterns due to this deficiency could not be significant. For a specific terrain topography, when

keeping β_P fixed and gradually increasing α_P, the overall predicted precipitation increases, but the spatial pattern of precipitation remains relatively stable (Figure S1a). When keeping α_P fixed and gradually increasing β_P, the model predicts an enhanced localization of precipitation on the windward side, but the average precipitation intensity over a large area remains relatively stable (Figure S1b). However, regardless of the values of α_P and β_P, the location with the maximum precipitation on the windward side remains unchanged. Therefore, the parameter β_P reflects the sensitivity of precipitation to changes in elevation and slope, while α_P is related to the average precipitation on a large scale. If we assume that the average precipitation over the low-lying plains in front of the mountain ranges (with near-zero elevation and slope) is P_0 , which can also represent the average precipitation on a large scale (or over the entire model domain), then

$$\alpha_P = \frac{P_0}{e_{sat}(T_0)} \quad (14)$$

where $e_{sat}(T_0)$ is the saturation vapor pressure at sea level. Thus, Equation (9) in the main text can be rewritten as

$$P = \left(\frac{P_0}{e_{sat}(T_0)} + \beta_P S\right) e_{sat}(T) \quad (15)$$

In the eastern Himalayan syntaxis, Anders et al. (2006) obtained the values of α_P and β_P through regression analysis, which are approximately 0.014 and 0.216, respectively. These set of values produced prediction that successfully captures the main characteristics of the current precipitation in the eastern Himalayan syntaxis, but failed to predict the maximum precipitation totals (the predicted value $P_{\max\_pred} = 3.5\ m/yr$, and the actual value $P_{\max\_actu} = 6\ m/yr$). To address this limitation, let's assume that the pattern of precipitation in the eastern Himalayan syntaxis strictly follows the model described in Equation (9) in the main text. We also assume the existence of true α_P and β_P in the syntaxis. The parameter values estimated by Anders et al. (2006) are denoted as $\alpha_P{}'$ and $\beta_P{}'$. Furthermore, let's consider that at the location where the maximum precipitation happens, the elevation, the topographic slope and the corresponding saturation vapor pressure are h_1, S_1, and $e_{sat}(h_1)$, respectively, then

$$P_{\max\_actu} = \alpha_P e_{sat}(h_1) + \beta_P S_1 e_{sat}(h_1) \quad (16)$$

Based on the above discussion, for a specific topography, the location with maximum precipitation remains relatively stable. Therefore, we have

$$P_{\max\_pred} = \alpha_P{}' e_{sat}(h_1) + \beta_P{}' S_1 e_{sat}(h_1) \quad (17)$$

Assuming $k_0 = P_{\max\_actu}/P_{\max\_pred}$, by combining equations (16) and (17), we obtain $\alpha_P = k_0\alpha_P{}' = 0.024$ and $\beta_P = k_0\beta_P{}' = 0.370$. Here, $\alpha_P = 0.024$ corresponds to precipitation of 1.019 m/yr in the low-lying plain in front of the mountain range (P_0). This predicted value is closer to the actual value in the eastern Himalayan syntaxis region compared to the estimated value of 0.594 m/yr using $\alpha_P = 0.014$ (Anders et al., 2006; Bookhagen & Burbank, 2006), indicating that such a correction is reasonable.

In this study, α_P is calculated based on various given average precipitation P_0 and Equation (14), while β_P is set to 0.370. The variation in the average precipitation intensity across the entire mountain range is achieved by adjusting the value of P_0.

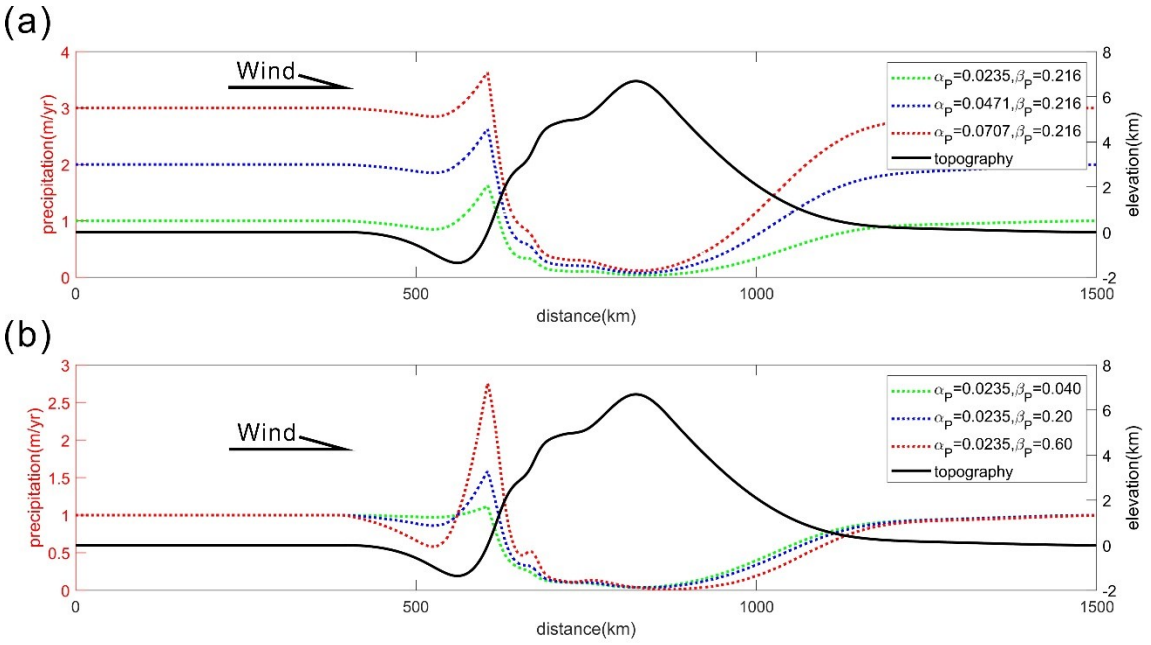

Figure S1. Sensitivity of predicted precipitation to the parameters α_P and β_P based on Equation (9) in the main text. (a) shows the predicted precipitation with fixed β_P and varying α_P, while (b) shows the predicted precipitation with fixed α_P and varying β_P. The solid black line represents the topography of an assumed mountain range, while the dashed green, blue, and red lines represent the predicted precipitation based on the topography and the orographic precipitation model as described in Equation (9) in the main text. It's assumed that the moisture-laden winds arrive from the left in both (a) and (b).

Table S1. Material properties used in the numerical experiments.

Properties	Sediments	Normal rock sequence	Decollement layer	Backstop
Flow law	Wet quartzite	Wet quartzite	Wet quartzite	quartzite
A_D(MPa^{-n} s^{-1})	3.2×10^{-4}	3.2×10^{-4}	3.2×10^{-4}	6.7×10^{-6}
n	2.3	2.3	2.3	2.4
Ea(kJ mol^{-1})	154	154	154	156
Va(cm^3)	0	0	0	0
$\rho_{0\ (solid)}$ (kg m^{-3})	2700	2700	2700	2700
$\rho_{0\ (molten)}$ (kg m^{-3})	2400	2400	2400	2400
σ_c(Pa)	1×10$^{7-6}$	1×10$^{7-6}$	1×10$^{5-4}$	1×10$^{7-6}$
γ_{int}	0.20-0.10	0.30-0.15	0.10-0.05	0.40-0.20
μ(GPa)	10	10	10	10
k(W m^{-1}K^{-1}, at T_K)	0.64+807/(T+77)	0.64+807/(T+77)	0.64+807/(T+77)	0.64+807/(T+77)

$T_{solidus}$(K, at P_{MPa})	889+17900/(P+54)+ 20200/(P+54)^2 at P<1200 MPa, 831+0.06P at P>1200 MPa	889+17900/(P+54)+ 20200/(P+54)^2 at P<1200 MPa, 831+0.06P at P>1200 MPa	889+17900/(P+54)+ 20200/(P+54)^2 at P<1200 MPa, 831+0.06P at P>1200 MPa	889+17900/(P+54)+ 20200/(P+54)^2 at P<1200 MPa, 831+0.06P at P>1200 MPa
$T_{liquidus}$(K, at P_{MPa})	1262+0.09P	1262+0.09P	1262+0.09P	1262+0.09P
Q_L(kJ kg^{-1})	300	300	300	300
H_r(μWm^{-3})	2.0	2.0	2.0	2.0
C_p(J kg^{-1}K^{-1})	1000	1000	1000	1000
α(K^{-1})	3×10^{-5}	3×10^{-5}	3×10^{-5}	3×10^{-5}
β(Pa^{-1})	1×10^{-11}	1×10^{-11}	1×10^{-11}	1×10^{-11}

Note. A_D, n, E_a and V_a are the flow law parameters, corresponding to material constant, stress exponent, activation energy, and activation volume, respectively (Ranalli, 1995). $\rho_{0\,(solid)}$ and $\rho_{0\,(molten)}$ are the standard densities of solid and molten rock, respectively. Strain weakening is applied within a plastic strain interval of 0–1, at which the compressive strength(σ_c) and internal friction coefficient(γ_{int}) decrease gradually. Q_L and H_r are the latent and radioactive heat production, respectively, μ is the shear modulus (Bittner & Schmeling, 1995; Turcotte & Schubert, 2014), k is thermal conductivity (Clauser & Huenges, 1995), $T_{solidus}$ and $T_{liquidus}$ are the wet solidus and dry liquidus temperatures of the considered rock, respectively (Schmidt & Poli, 1998), C_p is isobaric heat capacity, α is thermal expansion, β is compressibility.

Table S2. Numerical experiment summary with an initial geothermal gradient of 30 ℃ /km.

Convergence rate (cm/yr) / Average precipitation (m/yr)	0.5	1.0	1.5	2.0	2.5	3.0	3.5	4.0	4.5	5.0
0	S001	S002	S003	S004	S005	S006	S007	S008	S009	S010
2	S011	S012	S013	S014	S015	S016	S017	S018	S019	S020
4	S021	S022	S023	S024	S025	S026	S027	S028	S029	S030
6	S031	S032	S033	S034	S035	S036	S037	S038	S039	S040
8	S041	S042	S043	S044	S045	S046	S047	S048	S049	S050
10	S051	S052	S053	S054	S055	S056	S057	S058	S059	S060
12	S061	S062	S063	S064	S065	S066	S067	S068	S069	S070
14	S071	S072	S073	S074	S075	S076	S077	S078	S079	S080
16	S081	S082	S083	S084	S085	S086	S087	S088	S089	S090
18	S091	S092	S093	S094	S095	S096	S097	S098	S099	S100
20	S101	S102	S103	S104	S105	S106	S107	S108	S109	S110

Table S3. Numerical experiment summary with an initial geothermal gradient of 25 ℃ /km.

Convergence rate (cm/yr) / Average precipitation (m/yr)	0.5	1.0	1.5	2.0	2.5	3.0	3.5	4.0	4.5	5.0
0	S111	S112	S113	S114	S115	S116	S117	S118	S119	S120
2	S121	S122	S123	S124	S125	S126	S127	S128	S129	S130
4	S131	S132	S133	S134	S135	S136	S137	S138	S139	S140
6	S141	S142	S143	S144	S145	S146	S147	S148	S149	S150
8	S151	S152	S153	S154	S155	S156	S157	S158	S159	S160
10	S161	S162	S163	S164	S165	S166	S167	S168	S169	S170
12	S171	S172	S173	S174	S175	S176	S177	S178	S179	S180
14	S181	S182	S183	S184	S185	S186	S187	S188	S189	S190
16	S191	S192	S193	S194	S195	S196	S197	S198	S199	S200
18	S201	S202	S203	S204	S205	S206	S207	S208	S209	S210
20	S211	S212	S213	S214	S215	S216	S217	S218	S219	S220

Table S4. Additional numerical experiments with a convergence rate of 2 cm/yr.

Initial geothermal gradient(℃/km) / Average precipitation (m/yr)	10	15	20	35	40	45
2	ST01	ST02	ST03	ST04	ST05	ST06
6	ST07	ST08	ST09	ST10	ST11	ST12

References

Anders, A. M., Roe, G. H., Hallet, B., Montgomery, D. R., Finnegan, N. J., & Putkonen, J. (2006). Spatial patterns of precipitation and topography in the Himalaya. *Special Papers-Geological Society of America*, *398*, 39.

Bittner, D., & Schmeling, H. (1995). Numerical Modelling of Melting Processes and Induced Diapirism In the Lower Crust. *Geophysical Journal International*, *123*(1), 59-70. https://doi.org/10.1111/j.1365-246X.1995.tb06661.x

Bookhagen, B., & Burbank, D. W. (2006). Topography, relief, and TRMM‐derived rainfall variations along the Himalaya. *Geophysical Research Letters*, *33*(8).

Burg, J.-P., & Gerya, T. V. (2005). The role of viscous heating in Barrovian metamorphism of collisional orogens: thermomechanical models and application to the Lepontine Dome in the Central Alps. *Journal of Metamorphic Geology*, *23*(2), 75-95. https://doi.org/https://doi.org/10.1111/j.1525-1314.2005.00563.x

Clauser, C., & Huenges, E. (1995). Thermal conductivity of rocks and minerals. *Rock physics and phase relations: a handbook of physical constants*, *3*, 105-126.

Gerya, T. (2019). *Introduction to numerical geodynamic modelling*. Cambridge University Press.

Gerya, T. V., & Yuen, D. A. (2003). Rayleigh–Taylor instabilities from hydration and melting propel 'cold plumes' at subduction zones. *Earth and Planetary Science Letters*, *212*(1), 47-62. https://doi.org/https://doi.org/10.1016/S0012-821X(03)00265-6

Pinkerton, H., & Stevenson, R. J. (1992). Methods of determining the rheological properties of magmas at sub-liquidus temperatures. *Journal of Volcanology and Geothermal Research*, *53*(1), 47-66. https://doi.org/https://doi.org/10.1016/0377-0273(92)90073-M

Ranalli, G. (1995). *Rheology of the Earth*. Springer Science & Business Media.

Schmidt, M. W., & Poli, S. (1998). Experimentally based water budgets for dehydrating slabs and consequences for arc magma generation. *Earth and Planetary Science Letters*, *163*(1), 361-379. https://doi.org/https://doi.org/10.1016/S0012-821X(98)00142-3

Turcotte, D., & Schubert, G. (2014). Geodynamics.